Conference paper

Yoshifumi Sakaguchi*, Hidehito Asaoka and Maria Mitkova

Kinetics of silver photodiffusion into amorphous S-rich germanium sulphide – neutron and optical reflectivity

https://doi.org/10.1515/pac-2019-0217

Abstract: Silver photodiffusion is one of the attractive photo-induced changes observed in amorphous chalcogenides. In this research, we focus on amorphous S-rich germanium sulphide and study the kinetics of the silver photodiffusion by neutron reflectivity, as well as optical reflectivity. It was found from the neutron reflectivity profiles with 30 s time resolution that silver dissolved into the germanium sulphide layer, forming a metastable reaction layer between the Ag and the germanium sulphide layers, within 2 min of light exposure. Subsequently, silver slowly diffused from the metastable reaction layer to the germanium sulphide host layer until the Ag concentration in both layers became identical, effectively forming one uniform layer; this took approximately 20 min. Optical reflectivity reveals the electronic band structure of the sample, complementary to neutron reflectivity. It was found from the optical reflectivity measurement that the metastable reaction layer was a metallic product. The product could be Ag_8GeS_6-like form, which is regarded as the combination of GeS_2 and Ag_2S, and whose backbone is composed of the GeS_4 tetrahedral units and the S atoms. We attribute the first quick diffusion to the capture of Ag ions by the latter S atoms, which is realised by the S–S bond in amorphous S-rich germanium sulphide, while we attribute the second slow diffusion to the formation of the Ag–Ge–S network, in which Ag ions are captured by the former GeS_4 tetrahedral units.

Keywords: amorphous chalcogenide; neutron reflectivity; silver photodiffusion; SSC-2018.

Introduction

Silver photodiffusion is one of the various photo-induced changes observed in amorphous chalcogenides [1, 2]. The phenomenon was discovered by Kostyshin et al. and reported in 1966 [3]. The exposure of the silver and amorphous chalcogenide bi-layer films to visible light or ultra-violet light leads to the dissolution and diffusion of silver into the chalcogenide layer. Silver photodiffusion induces substantial changes in the physical and chemical properties, and there are potential applications such as photo-resist [4], fabrication of interference gratings [5, 6], and optical waveguides [6]. Recent interest in the phenomenon may be attributed to the technological potential of non-volatile memory Programmable Metallization Cell (PMC) devices, wherein silver photo-diffused films are used as solid-state electrolytes [7, 8]. To improve the performance of these devices, it is necessary to understand the movement of silver ions in the chalcogenide layer. In this respect, studies on the kinetics of silver photodiffusion will be helpful for controlling the movement of silver

Article note: A collection of invited papers based on presentations at the 13th International Conference on Solid State Chemistry (SSC-2018), Pardubice, Czech Republic, September 16–21, 2018.

***Corresponding author: Yoshifumi Sakaguchi,** Comprehensive Research Organization for Science and Society, Neutron Science and Technology Center, Tokai, Japan, e-mail: y_sakaguchi@cross.or.jp
Hidehito Asaoka: Japan Atomic Energy Agency, Advanced Science Research Center, Tokai, Japan
Maria Mitkova: Boise State University, Electrical and Computer Engineering, Boise, ID, USA

ions more efficiently. In fact, photo-doped silver ions into a chalcogenide layer exhibit anomalous diffusion, and investigation on the kinetics of silver photodiffusion is of great interest. Hitherto, the changes in the depth profile of a Ag/chalcogenide bi-layer film during a light exposure were investigated primarily through Rutherford backscattering (RBS) [9–15]. According to their results, the Ag ion concentration does not decrease gradually in the depth direction, with an exponential decay curve; however, it abruptly reduces at a certain point, showing a step-like profile. This implies that the movement of silver photodiffusion is not due to a difference in concentration, but due to a particular type of reaction that occurs at the interface.

However, it was difficult to perform *in situ* measurements to ascertain the depth profile during the light exposure, because strong X-rays, ion beams, and electron beams can induce silver diffusion by the probe beams [9, 10, 16]. For instance, Yamamoto et al. [9] noted the influence of a He^+-ion beam on the silver photodiffusion into As_2S_3 glasses. They used 350 keV He^+ beams and reported the dose limit as $1.35\times10^{14}/cm^2$. Rennie et al. [10] also indicated the ion beam effect on Ag/amorphous $GeSe_2$ films, using a 2 MeV He^+ beam with an overall charge in the range of 0.5–1.0 $\mu C/mm^2$. Recently, we focused on neutron beams, which do not induce silver diffusion and performed time-resolved neutron reflectivity measurements to investigate the kinetics of silver photodiffusion into Ge chalcogenide [17–23]. Neutron reflectometry is a powerful *non-destructive* technique to explain the structure of multi-layers in thin films, giving precise understanding of their thickness and roughness with an angstrom scale, and the technique is applicable to a time-dependent phenomenon under a light exposure. Based on the measurements of the Ag/Ge chalcogenide films, it was found that the kinetics significantly depended upon the Ge composition and the thickness of chalcogenide. These examples of kinetics dependences are very interesting because they can be utilised in controlling ion movement for applications such as PMC devices. In this experiment we focus on amorphous S-rich germanium sulphide and study the kinetics of silver photodiffusion into the layer by neutron reflectivity along with optical reflectivity. In fact, we have already reported a preliminary result of neutron reflectivity measurement of a $Ag/Ge_{20}S_{80}/Si$ substrate under a light exposure [17]. However, a detailed analysis was not performed. In this study, we demonstrate the time evolution of the layer structure of a $Ag/Ge_{20}S_{80}/Si$ substrate, including the information on the thickness and the Ag concentration, based on the detailed analysis of the result. In addition, we performed the optical reflectivity measurement of a $Ag/Ge_{25}S_{75}/Si$ substrate. Optical reflectivity reflects the electronic band structure of the sample and can provide a complementary information to the neutron reflectivity from which thicknesses and densities of the layers are obtained. We expect from the optical reflectivity measurement that the change of the metallic nature by silver photodiffusion will be demonstrated. Kinetics of silver photodiffusion into amorphous S-rich germanium sulphide layer is discussed based on these experimental results.

Experimental

The neutron reflectivity of a thin film can be calculated by applying the theory of optics [24]. It is obtained by providing the wavelength (λ) and the incident angle or scattering angle (θ) of the beam, as well as the refractive index (n) and the thickness of the film [25–27]. In neutron reflectivity, the refractive index is denoted as:

$$n \sim 1 - \frac{\beta \lambda^2}{2\pi}$$

where β is the scattering length density (SLD) of the sample. For the compound made of N types of atoms, β is calculated as:

$$\beta = \frac{\rho N_A \sum_{i=1}^{N} c_i b_i}{\sum_{i=1}^{N} c_i M_i}$$

where ρ is the mass density of the bulk, N_A is the Avogadro number, c_i is the concentration for each element, b_i is the scattering length for each element, and M_i is the atomic molar mass for each element. The neutron reflectivity of a multi-layer film with an SLD profile in the depth direction is calculated by Parratt's recursive method or by Abeles matrix method as well as X-ray reflectivity [25–31]. The measured neutron reflectivity is compared to

the calculated neutron reflectivity obtained from a model of the SLD depth profile, and accordingly, the model is evaluated. Furthermore, curve fitting is performed to identify the appropriate parameters, such as the thicknesses and the SLDs. When selecting a proper model of the SLD depth profile is difficult, Fourier transform analysis can be helpful [32, 33]. The peak positions indicate the thicknesses of the layers in the film, including the sum of the thicknesses. Although the Fourier transform profile does not indicate the order of layers, time evolution of the profile is very useful in the present study because the thickness of a layer (considering the Ag layer) changes by silver photodiffusion. The height of the Fourier transform also provides important information on the layer structure of a film [22], and it is related to a difference in the SLD at the interface.

Neutron reflectivity measurements were performed on BL17 (*SHARAKU*) [34] at the Materials and Life Science Experimental Facility (MLF) of the Japan Proton Accelerator Research Complex (J-PARC). J-PARC is the research complex providing the intensive proton beams used for the research [35]. The 3 GeV proton beam hits the liquid mercury target in the MLF, generating pulsed neutron beams through nuclear spallation reactions [27, 36] at 25 Hz. In the present experiment, the proton beam power was 300 kW. White light from a 300 W xenon lamp (MAX-303, ASAHI Spectra, Co., Ltd., Japan) was used as the excitation light source, and the exposure of the sample was controlled by the facility-wide device control system, called IROHA [37]. The spectral range of the excitation light source through the ultra-violet-type mirror module was from 250 to 430 nm. The power of the light at the sample position was approximately 37 mW/cm^2. Considering the spectrum of the light source [38] and the absorption coefficients of amorphous $Ge_{20}S_{80}$ [39], the photon density *per se*cond absorbed by a $Ge_{20}S_{80}$ 1500 Å film is estimated to be 1.7×10^{16} photons/s · cm^2. The optical gap of amorphous $Ge_{20}S_{80}$ is 2.77 eV (448 nm) [39] and a light with an energy greater than the optical gap is used for silver photodiffusion. The neutron reflectivity (R) was obtained by $R=I/I_0$, where I is the intensity of the reflected beam and I_0 is the intensity of the incident beam as a function of neutron time-of-flight (TOF), t_{TOF}. I_0 was obtained by measuring the intensity of the direct beam without taking the sample into consideration. The TOF was converted to the wave vector transfer, Q, by using the following relationships: $\lambda=h\ t_{TOF}/mL$, where λ is the neutron wavelength, h is Planck's constant, m is the mass of a neutron, L is the length between the neutron source and the detector, and $Q=\ 4\pi\ \sin\ \theta\ /\lambda$ where $\theta=\theta_i$ (incident angle) $=\theta_f$ (scattering angle). Prior to the exposure of light, TOF spectra were measured at two different angles, 0.4° and 0.8°, respectively, and these spectra were combined to give a static single spectrum over a wide Q range. During the light exposure, the sample was positioned at an angle of 0.4°, and the time evolution of the transient TOF spectrum was measured while exposing the sample to light from the xenon lamp. In the measurement, the slits were set to $\Delta\theta/\theta=5\,\%$. The details of the experimental procedure are shown in Ref. 19. At the MLF, neutron data are acquired using an event recording system in which every detected neutron is labelled with the neutron pulse number, time taken from a standard clock used across the facility, and TOF [37, 40]. From the complete recorded data set, arbitrarily time-sliced TOF spectra were obtained using the data reduction system of the facility. The obtained neutron reflectivity profiles were fitted using the Motofit package [41].

Optical reflectivity is measured by using a tungsten lamp, a monochromator (PDP-320JL-K, Photon Design, Japan), and a photo-multiplier (R374, Hamamatsu Photonics, Japan). Initially, we measured the square of the absolute reflectivity of an aluminium-coated mirror by rectifying the reflection from the optical bending mirrors through which a probe light beam passed during the reflectivity measurement [42]. Subsequently, we measured the reflectivity spectrum of the sample, and obtained the absolute optical reflectivity of the samples by referring to the reflectivity data from the aluminium-coated mirror.

Results and discussion

Neutron reflectivity

Saturated photo-induced changes after 71 min of light exposure –static neutron reflectivity measurement

Figure 1 shows the static neutron reflectivity profiles (R–Q) of the Ag 500 Å/$Ge_{20}S_{80}$ 1500 Å/Si substrate before and after 71 min of light exposure. Figure 2 presents the Fourier transforms of RQ^4. The peak position indicates

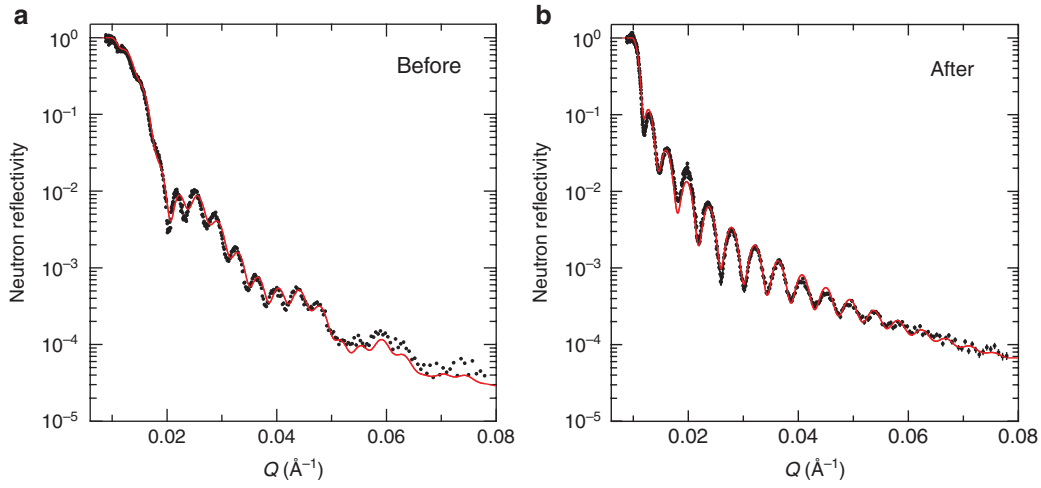

Fig. 1: Neutron reflectivity profiles (R–Q) of the Ag 500 Å/$Ge_{20}S_{80}$ 1500 Å/Si substrate. (a) Before light exposure, (b) after 71 min of light exposure.

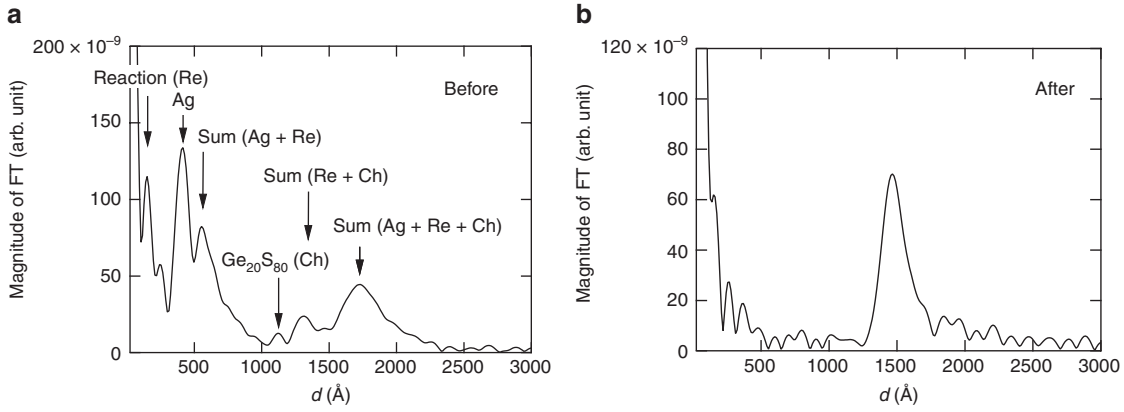

Fig. 2: Fourier transforms of RQ^4. (a) Before the light exposure, (b) after 71 min of light exposure.

the thickness of a layer in the film. In general, there are ${}_{n+1}C_2=(n+1)\ n/2$ peaks for a multi-layer film with n layers [22, 33]. For instance, there is 1 peak that represents a film with 1 layer, 3 peaks that represent a film with 2 layers, and 6 peaks that represent a film with 3 layers. Figure 2a illustrates 6 peaks. This indicates that the film has 3 layers, and suggests that there is a reaction layer "before" the light exposure. We infer that the reaction layer was thermally produced during the process of thermal evaporation owing to the sensitive reactivity of the $Ge_{20}S_{80}$ surface. Following 71 min of light exposure, 1 peak is observed in the Fourier transform. This indicates that the film has only 1 layer and suggests that the film changed to form one uniform layer by silver photodiffusion. Figure 3 shows the SLD profiles of the Ag 500 Å/$Ge_{20}S_{80}$ 1500 Å/Si substrate before and after 71 min of light exposure. The SLD profiles are the result of curve fitting on the experimental neutron reflectivity data. The neutron reflectivity curves calculated from the SLD models are indicated in red in Fig. 1. The calculated reflectivity curves agree well with the experimental data. The SLD value of one uniform layer following the light exposure is 2.1×10^{-6} Å^{-2}, which is between the values for Ag (4.7×10^{-6} Å^{-2}) and $Ge_{20}S_{80}$ (1.7×10^{-6} Å^{-2}). This is consistent with our expectation that Ag ions are introduced into the $Ge_{20}S_{80}$ layer. In the case of the film that has undergone 71 min of light exposure, a vacant region is observed between the film and the substrate. A similar region was also observed for silver photodiffusion into $Ge_{33}S_{67}$ [21] after an extended duration of light exposure. We infer that silver photodiffusion was completed in the film and that the interaction between the reaction layer and the Si substrate caused a type of separation between them.

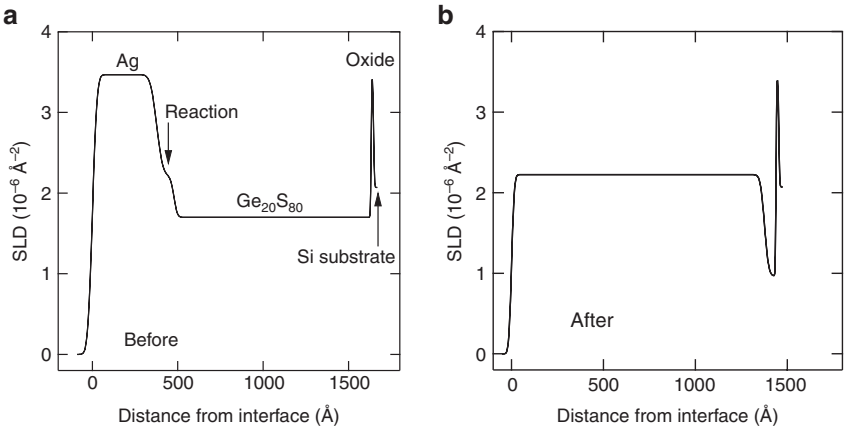

Fig. 3: SLD profiles of the Ag 500 Å/$Ge_{20}S_{80}$ 1500 Å/Si substrate. (a) Before the light exposure, (b) after 71 min of light exposure.

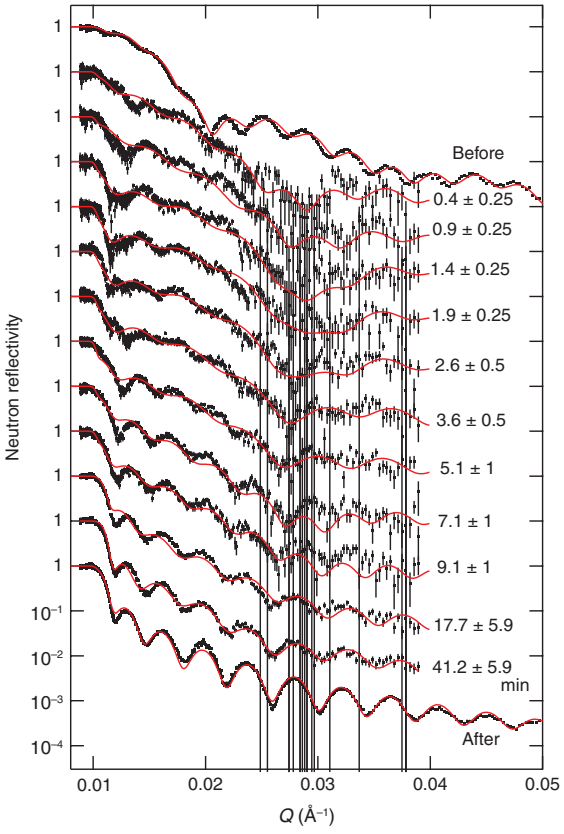

Fig. 4: Time evolution of neutron reflectivity profiles (R–Q) of the Ag 500 Å/$Ge_{20}S_{80}$ 1500 Å/Si substrate during 71 min of light exposure and in the subsequent time period.

Photo-induced changes during light exposure-time-resolved neutron reflectivity measurement

Figure 4 shows the time evolution of the neutron reflectivity profiles (R–Q) of the Ag 500 Å/$Ge_{20}S_{80}$ 1500 Å/Si substrate during 71 min of light exposure. It is noted that the neutron reflectivity profiles are plotted with a time resolution of 30 s (±0.25 min) in the initial 2 min, and that substantial changes are observed. The change in the neutron reflectivity profile is very quick: the shape of the neutron reflectivity profile at 0.4 min completely differs from the shape before the light exposure. Figure 5a shows the time evolution of the Fourier

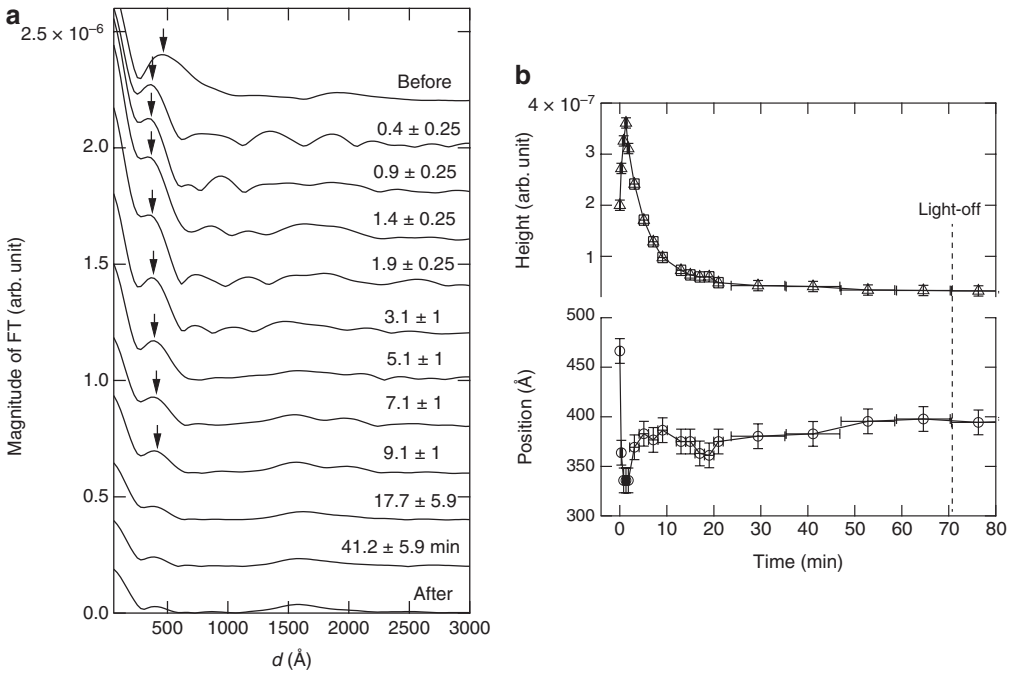

Fig. 5: (a) Time evolution of Fourier transform of RQ^4 of the Ag 500 Å/$Ge_{20}S_{80}$ 1500 Å/Si substrate during 71 min of light exposure. The first peak positions are indicated by arrow signs. (b) Time variations of the position and the height of the first peak.

transform of RQ^4. The Fourier transformation was performed using the neutron reflectivity in $0.008 < Q < 0.04$ Å^{-1} range, which was obtained at only one fixed angle, $\theta = 0.4°$. Because of this limitation, the peak is broader compared with the peak in Fig. 2, in which neutron reflectivity in wider Q range ($0.008 < Q < 0.08$ Å^{-1}) is used.

The time variations of the first peak position and its height are shown in Fig. 5b. In both plots, there are two processes. In the first process (0–2 min), the peak position quickly decreases while its height quickly increases. In the second process (2–20 min), the peak position increases while its height decreases. We infer from the thickness resolution that the peaks of the Ag layer and that of the reaction layer overlap with each other in the first peak. Assuming this situation, the scenario of silver photodiffusion in this system is as follows. The Ag layer becomes thinner by diffusing the Ag into the $Ge_{20}S_{80}$ layer and disappearing at the early stage of the reaction process within 2 min. The reaction layer grows from an initial thickness of 100 Å immediately after light exposure. However, following the quick growth, its thickness is retained at a near constant value of approximately 350 Å.

Hitherto, a similar two-stage reaction was observed in the modified optical reflectivity of Ag/$As_{33}S_{67}$, measured by Wagner et al. [15, 43, 44]. They also measured RBS for the films with different light exposure times, and concluded the kinetics in the depth direction. (1) The Ag layer disappears and a uniform reaction layer is formed in the vicinity of the surface, leaving a thinner and refined layer of $As_{33}S_{67}$, at the early stage of the reaction process. (2) Subsequently, the reaction layer becomes thicker with a longer duration of light exposure. (3) Finally, the film becomes one uniform reaction layer [14, 15]. In other words, there is a *diffusion front*, indicating a step-like Ag concentration profile in the film, and this diffusion front progresses with light exposure time until the front reaches the interface between the chalcogenide film and Si substrate (the oxide layer). Assuming that silver photodiffusion occurs similarly in the present system, we would expect the following behaviour in the peak position. The peak of the Ag layer immediately shifts to the shorter distance side with time due to the silver dissolution and disappears at the early stage of the reaction process. The peak of the $Ge_{20}S_{80}$ layer gradually shifts toward the side at a shorter distance through the entire reaction process and disappears at the final stage of the reaction process. The peak of the reaction layer shifts to the side at a longer distance with light exposure time, and continues even after the reaction is completed. According to

the results of the static neutron reflectivity measurement in Fig. 3, the thickness of the initial reaction layer is 100 Å, whereas in the case of the saturated reaction layer, it is 1300 Å. Therefore, we would expect that the peak of the reaction layer shifts from 100 to 1300 Å during the light exposure. However, this change is not observed in Fig. 5a and b. This means that silver diffusion in this system does not follow the model of the progression of a diffusion front.

Although the Fourier transformation is a model-independent analytical technique, we have assumed the shrinkage and disappearance of the Ag layer in the first fast reaction process in the above discussion. Therefore, it is important to have evidence of this assumption. The Fourier transformation technique is based on a kinematic theory, wherein single-event scattering is assumed. This theory is not applicable near the critical edge for total external reflection. However, the critical wave vector transfer (the critical edge), Q_c, can be a good measure to show the characteristics of a film in the region. In general, Q_c is obtained by [25, 26]:

$$Q_c = 4\sqrt{\pi\beta}$$

For instance, Q_c of silver is estimated to be 1.32×10^{-3} (Å^{-1}), and that of $Ge_{20}S_{80}$ is estimated to be 9.24×10^{-2} (Å^{-1}). In the process of silver photodiffusion, we would expect a considerable shift of Q_c according to the disappearance of the Ag layer. In the present work, we define Q_c experimentally as the Q point where an RQ^4 curve drops, deviating from a Q^4 curve. In the total external reflection region, an RQ^4 curve lies on Q^4 because $R=1$. In the Q region where kinematic theory is applicable, an RQ^4 curve oscillates around a constant value, because R decays with Q^{-4} according to kinematic theory. The result is presented in Fig. 6a. Before the light exposure, the RQ^4 curve drops on two instances. This means that there are two $Q_c s$: one for the Ag layer, and the other for the reaction layer. Time variations of the $Q_c s$ are presented in Fig. 6b. The Q_c of the Ag layer disappears within 1 min. This suggests that the Ag layer disappears in this time region. The Q_c of the reaction layer slightly shifts toward the lower side of Q until 10 min. This could be related to the decrease in the SLD due to a transfer of Ag ions from the reaction layer to the $Ge_{20}S_{80}$ host layer.

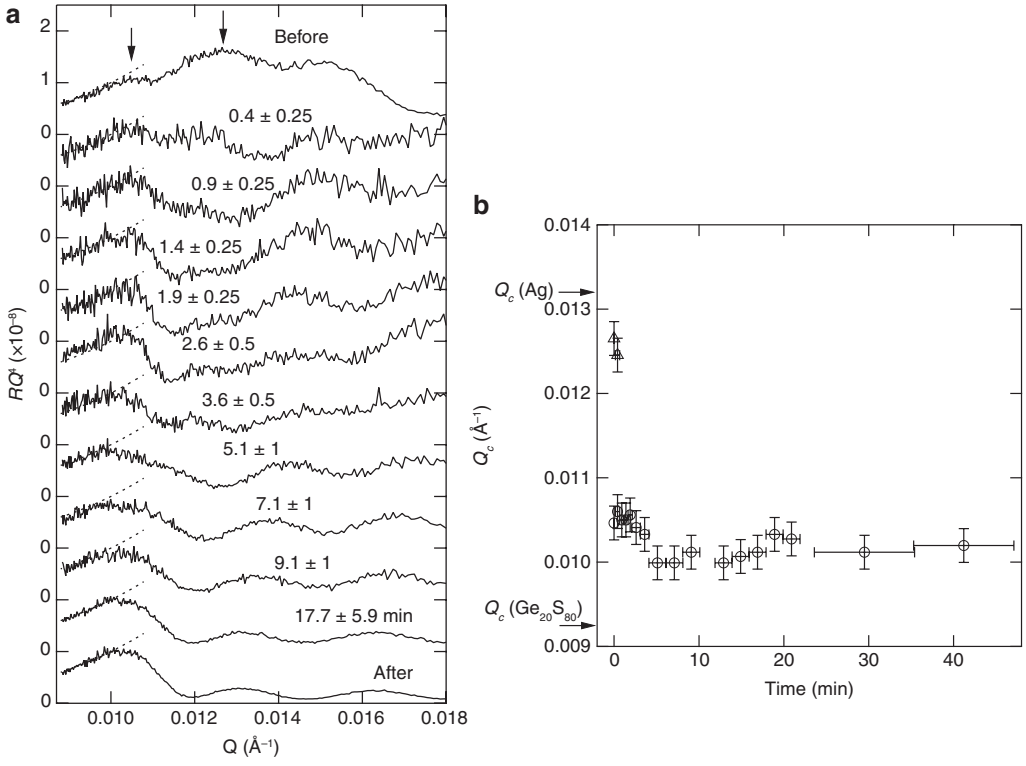

Fig. 6: (a) Time evolution of RQ^4. Dotted curves indicate $y=Q^4$ [RQ^4 ($R=1$)]. Neutron reflectivity in the total reflection region ($R=1$) follows the curve. (b) Time variation of the critical wave vector transfer, Q_c.

Based on the results of the Fourier transform and the critical edge, curve fitting was performed for the time-resolved neutron reflectivity profiles. In the fitting, we assumed the following: (1) the Ag layer becomes thinner and disappears in the first 2 min; (2) the reaction layer grows in the initial 2 min, but its thickness does not significantly change during the second reaction process (2 – 20 min); (3) the SLD of the reaction layer decreases and that of the $Ge_{20}S_{80}$ host layer increases during the second reaction. The time evolution of the SLD profile, which was obtained from the curve fitting, is shown in Fig. 7a. The fitted neutron reflectivity curves, illustrated in red (Fig. 4), are in accordance with the experimental data. Time variations of the fitting parameters, namely thickness and SLD, are shown in Fig. 7b. Essentially, the changes of the thickness and the SLD in the above assumptions were replicated in the changes of the fitting parameters. The layer of Ag disappears and the reaction layer grows in the initial 2 min, and the thickness of the reaction layer is retained at a constant value, 270 Å, in the second reaction. The SLD of the reaction layer decreases, and that of the $Ge_{20}S_{80}$ host layer increases, until both of the layers merge. Because all Ag ions present in the Ag layer with a thickness of 380 Å dissolve into the reaction layer with a thickness of 270 Å, the composition of the metastable reaction layer is estimated to be $Ag_{0.69}(Ge_{0.2}S_{0.8})_{0.31}$. The mass density is estimated to be 17.26 (g/cm^3), although it has uncertain density. In this case, the SLD should be 6.3×10^{-6} (Å^{-2}), which is inconsistent with the result of fitting, ~3.2×10^{-6} (Å^{-2}). Probably, a part of Ag ions reached the $Ge_{20}S_{80}$ host layer, and the actual content of Ag ions in the metastable reaction layer could be smaller than the estimation. Concerning the fully saturated reaction film, the composition is estimated to be $Ag_{0.34}(Ge_{0.2}S_{0.8})_{0.66}$. The mass density is estimated to be 5.14 (g/cm^3), which is logical considering the ternary compound [45]. From the composition and the mass density, the SLD is estimated to be 2.25×10^{-6} (Å^{-2}), which is consistent with the fitting result of the static neutron reflectivity shown in Fig. 3.

It is noted that there is a significant dip between the metastable reaction layer and the $Ge_{20}S_{80}$ host layer in the SLD profiles in the time region from 1.4 to 5 min. The dip signifies a larger difference in the SLD at the

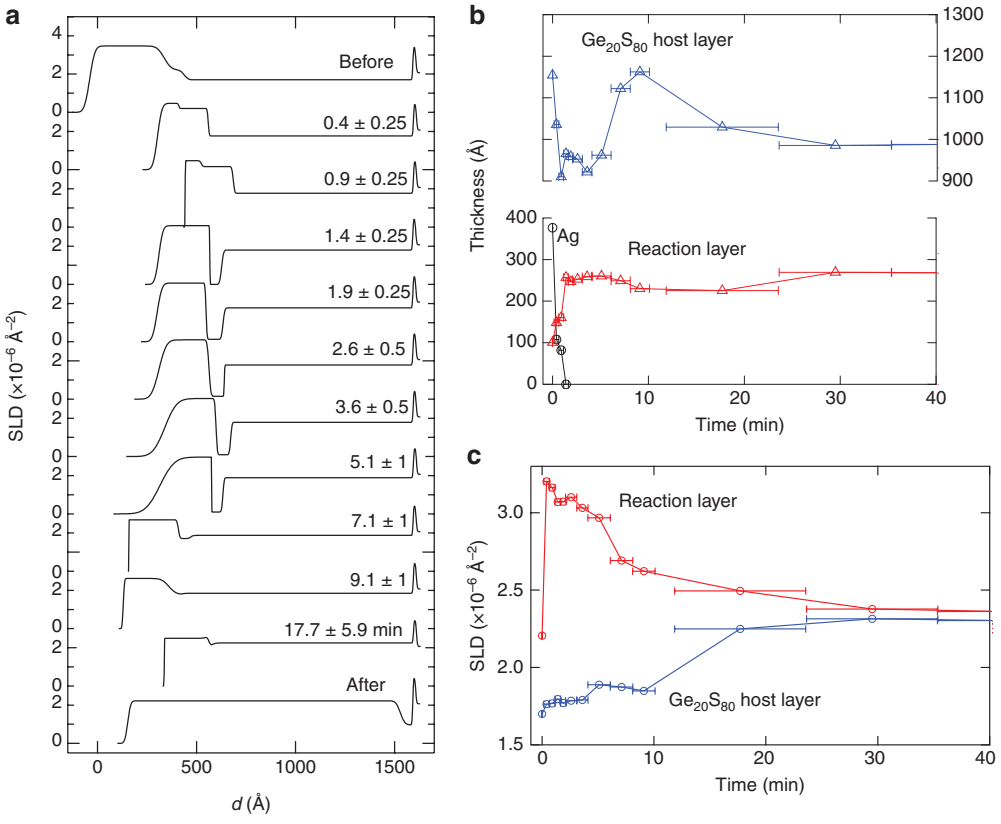

Fig. 7: (a) Time evolution of SLD profiles of the Ag 500 Å/$Ge_{20}S_{80}$ 1500 Å/Si substrate during 71 min of light exposure. (b) Time variations of the thicknesses of the Ag layer, the reaction layer, and the $Ge_{20}S_{80}$ host layer. (c) Time variations of the SLDs of the reaction layer and the $Ge_{20}S_{80}$ host layer.

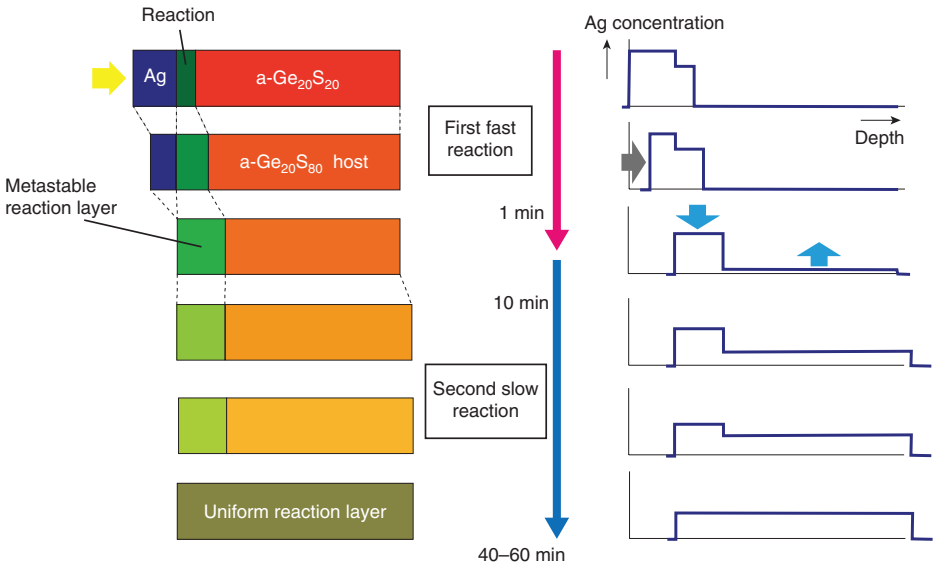

Fig. 8: (Left side) Schematic illustration of the time evolution of the layer structure by light exposure. (Right side) Time evolution of the Ag concentration profile in the depth direction.

interface between the metastable reaction layer and the $Ge_{20}S_{80}$ host layer, and this is consistent with the increase in the height of the first peak in the Fourier transform, as shown in Fig. 5b, which can be caused by an increase in the difference of the SLD at an interface [22]. Without assuming such a dip, fitting was not successful in the time region. We had also observed the dip in the Ag 500 Å/$Ge_{40}S_{60}$ 1500 Å/Si and Ag 500 Å/$Ge_{40}S_{60}$ 2000 Å/Si substrates during and after the light exposure [22]. For the films, we interpreted that the dip indicated a growth of Ag-diffused reaction domains on the interface plane between the Ag layer and the $Ge_{40}S_{60}$ host layer. We infer that this type of domain growth also occurs in the process of silver photodiffusion in the present film. In fact, Elliott proposed the formation of dendrites of photodoped reaction developed from grain-boundary nucleation sites in the metal in an induction period before the onset of fast photodissolution [46]. From surface observations using atomic force microscopy, Murakami and Wakaki also observed that the surface roughness increases with numerous narrow dips when a He–Cd laser illuminated the Ag/GeS_2 film [47]. If such inhomogeneous patterns are formed on the interface plane, a specular reflection from the depth region will be reduced, and the dip in the SLD profile can appear. Considering the result of the time variations of the thickness and the SLD (Fig. 7b), the kinetics of silver photodiffusion into $Ge_{20}S_{80}$ can be illustrated as presented in Fig. 8. In the initial quick reaction process, the Ag layer becomes thinner due to the Ag dissolution and a metastable Ag-doped reaction layer is formed in the vicinity of the interface between the Ag layer and the $Ge_{20}S_{80}$ layer. The maximum Ag concentration in the metastable reaction layer is approximately 70 %. In the second slow reaction process, Ag ions diffuse from the metastable reaction layer to the $Ge_{20}S_{80}$ host layer, resulting in the decrease in the Ag concentration in the metastable reaction layer, and the increase in the Ag concentration in the $Ge_{20}S_{80}$ host layer. When both Ag concentrations become equal, the layers merge to form one uniform reaction layer, and the reaction is completed. Hitherto, Wagner measured RBS of Ag/$Ge_{30}S_{70}$ with different illumination times [48]. Consequently, the diffusion front progresses as they observed in Ag/$As_{33}S_{67}$ films [14, 15]. Simultaneously, an additional Ag-rich region is formed in the vicinity of the surface. This is similar to the present result.

Optical reflectivity

In the above discussion, with respect to the SLD of the metastable reaction layer, the estimations from the thickness and the fitting result showed inconsistency. This could be caused by the assumption that *all* Ag

ions in the Ag layer are included in the metastable reaction layer. Assuming that a part of the Ag ions entered the $Ge_{20}S_{80}$ host layer, the model of the silver photodiffusion kinetics presented in the previous section is plausible. However, it is desirable to have a further knowledge about the metastable reaction layer, by using a complementary technique to ensure the model. Optical reflectivity reflects the electronic band structure of the surface of the sample, and can demonstrate significant changes from metallic to semiconducting one, by a photo-induced dissolution of metallic Ag layer. Therefore, we performed the optical reflectivity measurements using a weak probe light beam of a tungsten lamp, which does not induce silver diffusion. For the measurement, we used Ag 500 Å/$Ge_{25}S_{75}$ 1500 Å/Si substrate films. The neutron reflectivity of the films has already been measured [20]. The photo-induced changes in the neutron reflectivity profiles are complex, and

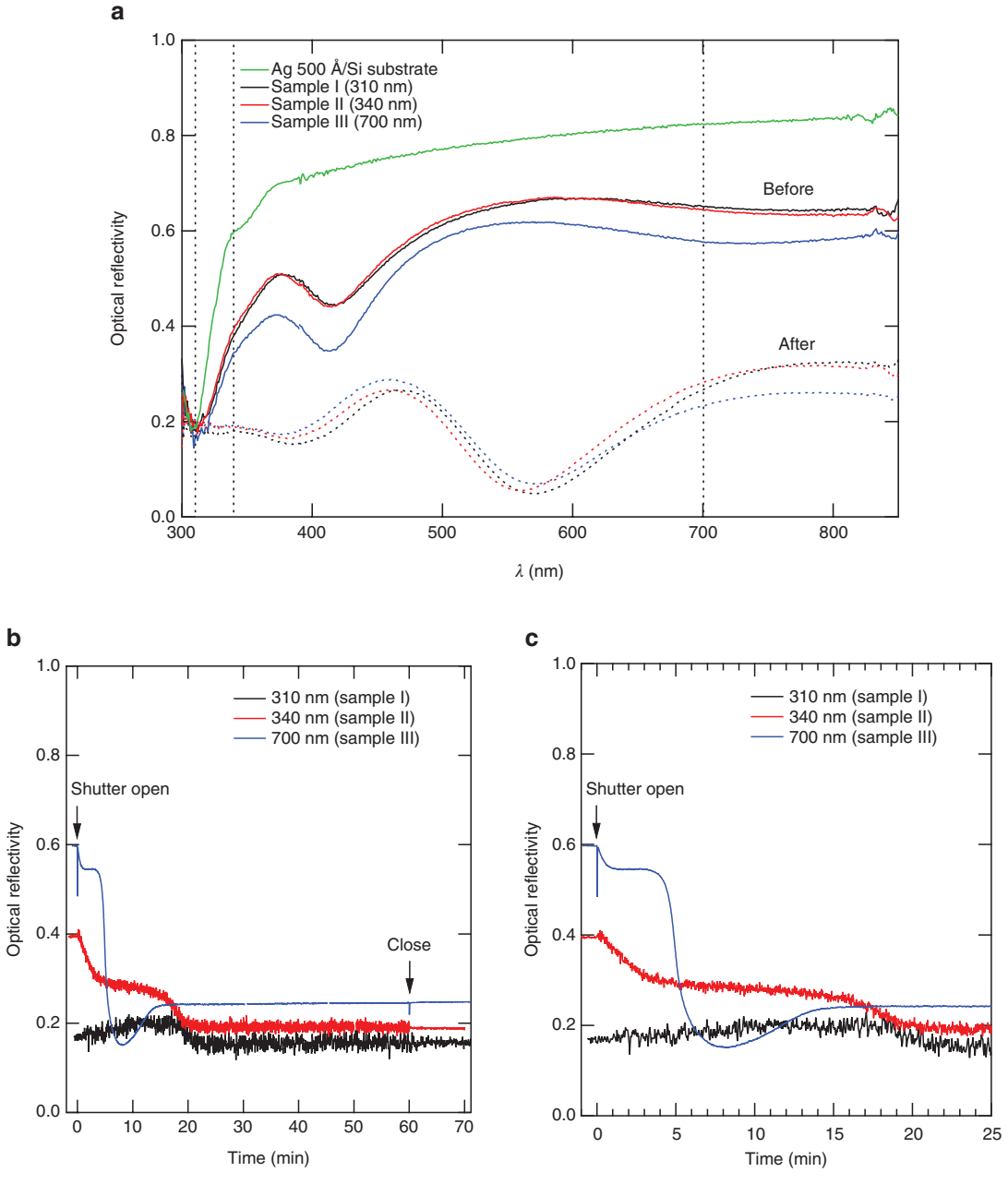

Fig. 9: (a) Optical reflectivity spectra of the Ag 500 Å/$Ge_{25}S_{75}$ 1500 Å/Si substrate before and after a 60 min light exposure. (b) Time variation of optical reflectivity of the Ag 500 Å/$Ge_{25}S_{75}$ 1500 Å/Si substrate at 310, 340, and 700 nm during the 60 min light exposure. (c) Enlarged figure of (b), focussing on the time region from 0 to 25 min.

the Fourier transformation analysis and the fitting were unsuccessful in the time region from 3 to 16 min. However, the formation of a metastable layer was expected on the $Ge_{25}S_{75}$ host layer, and silver diffusion was incomplete, while still leaving the bi-layer structure of the metastable reaction layer/$Ge_{25}S_{75}$ host layer. Initially, the chalcogenide sample was prepared as $Ge_{20}S_{80}$. However, we found from the static neutron reflectivity measurement that the SLD is greater compared to $Ge_{20}S_{80}$, and considered the sample as $Ge_{25}S_{75}$. The behaviour of the Q_c is similar compared to that in the present result (Fig. 6). The Q_c of the Ag layer disappears after approximately 2 min [20]. Therefore, the Ag dissolution and the formation of the metastable reaction layer in the film is expected to occur in the same manner as in the Ag/$Ge_{20}S_{80}$/Si substrate film.

Figure 9a shows the optical reflectivity spectra of the Ag 500 Å/$Ge_{25}S_{75}$ 1500 Å/Si substrate films before onset of light exposure and after 60 min of light exposure. In the optical reflectivity measurement, we used the excitation light source from the xenon lamp through the visible–type mirror module with the intensity distribution from 350 nm to 800 nm [38]. The power of the light at the sample position was approximately 210 mW/cm^2. The photon density per second absorbed by a $Ge_{25}S_{75}$ 1500 Å film is estimated to be 6.3×10^{15} photons/s · cm^2, considering the spectrum of the light source [38] and the absorption coefficients of amorphous $Ge_{25}S_{75}$ [39, 49]. This light source was also used for the neutron reflectivity measurement of the Ag 500 Å/$Ge_{25}S_{75}$ 1500 Å/Si substrate. In Fig. 9a, the optical reflectivity of the Ag 500 Å/Si substrate is also shown. The spectrum is comparable to the data in the literature [42] although there is a small difference, which would be caused by the difference in the thickness of the Ag film. The high reflectivity of the Ag 500 Å/Si substrate with approximately 0.8 in the wavelengths from 600 nm to 850 nm indicates the plasma reflectivity of metals, which is caused by free electrons in metals [50]. The high reflectivity (~0.6) of the Ag 500 Å/$Ge_{25}S_{75}$ 1500 Å/Si substrate in the wavelengths is attributed to the Ag layer on the surface. Fringes on the reflectivity curve of the Ag 500 Å/$Ge_{25}S_{75}$ 1500 Å/Si substrate before the light exposure is resulted from the optical interference by the $Ge_{25}S_{75}$ 1500 Å layer below the Ag layer. Following 60 min of light exposure, the reflectivity decreases down to 0.2, and a new fringe pattern appears, caused by the optical interference by the Ag-doped reaction layer. Time variation of the optical reflectivity for the monochromatized light beam at 700 nm is shown in Fig. 9b. Figure 9c is the enlarged figure of Fig. 9b, focussing on the time region from 0 to 25 min. The reflected intensity data were acquired every second. The reflectivity quickly decreases followed by opening the light shutter until 1 min, and subsequently, it is retained at a constant value of 0.54, which is a still high reflectivity, until 4 min. Subsequently, it decreases again to the level of 0.15, which is remarkably low to consider the film as a metal, until 8 min. Moreover, it increases up to 0.24 until 16 min, and followed by retaining the constant value, indicating the saturation of the photo-induced change. These changes are very similar compared to the critical edge observed in the Ag 500 Å/$Ge_{25}S_{75}$ 1500 Å/Si substrate films [20], and those in the present result as shown in Fig. 6b. From the result of the transient optical reflectivity, we infer that the following changes occur in the film. (I) 0 min to 1 min: Ag ions dissolve into the $Ge_{25}S_{75}$ layer from the Ag layer. (II) 1 min to 4 min: the Ag layer disappears and the metastable reaction layer is formed near the surface region. The metastable reaction product possesses metallic nature. (III) 4 min to 8 min: The Ag diffusion quickly progresses from the metastable reaction layer to the $Ge_{25}S_{75}$ host layer. As a result, a metallic reflection is lost from the film. (IV) 8 min to 16 min: The Ag diffusion occurred too much in process stage III. The Ag diffusion in the inverse direction occurs until the equilibrium condition is reached. In the reflectivity curve of the Ag 500 Å/Si substrate (Fig. 8a), there is a sharp absorption of approximately 310 nm. This is attributed to the transition from *d* states to the Fermi surface [51], and indicates the presence of the Ag layer. The peak is also observed in the Ag 500 Å/$Ge_{25}S_{75}$ 1500 Å/Si substrate before light exposure, and it is not observed after the light exposure. However, the reflectivity at 310 nm does not change substantially (approximately at 0.2), in the spectra before and after exposure. In the time variation during the light exposure, it increases to a small amount in the time from 0 min to 10 min, and quickly decreases in the time from 18 min to 23 min. These changes may be caused by the fringes, rather than the absorption peak at 310 nm. The fringes can change by the introduction of Ag ions into the reaction layer. The reflectivity at 340 nm quickly decreases in the time from 0 min to 4 min, and gradually decreases in the time from 4 min to 16 min, and subsequently, quickly decreases in the time from 16 min to 20 min. It seems that two factors, the fringes and the absorption peak at 310 nm, contribute to the reflectivity at 340 nm, and the interpretation of the time variation is partially difficult.

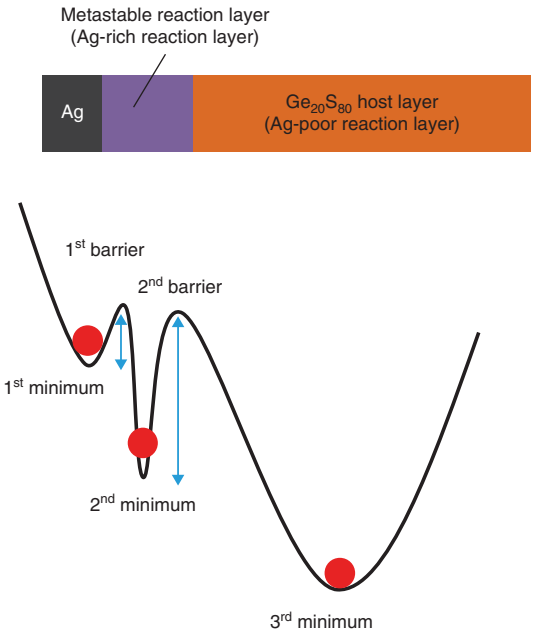

Fig. 10: Free energy curve that explains the silver photodiffusion into amorphous S-rich germanium sulphide.

It is concluded from the result of the optical reflectivity measurement that the Ag layer dissolves into the S-rich germanium sulphide layer, and disappears within 2 min after light exposure, and that a metastable reaction layer with metallic nature is formed in the time region.

Process of silver photodiffusion into S-rich germanium sulphide

The results of the neutron reflectivity and the optical reflectivity can be comprehended using a free-energy curve presented in Fig. 10. There are three potential minima and two potential barriers. The first minimum state is the highest among the three minima in terms of the energy level and corresponds to the Ag layer. By a light exposure with greater energy than the first barrier, which is between the first minimum and the second minimum, a state changes to be the second minimum. This corresponds to the temporarily existing metastable reaction layer, wherein a considerable amount of Ag ions is contained. With a continuous light exposure, a state moves to the third minimum, for which energy is the lowest among the three potential minima, by overcoming the second barrier. This change corresponds to the Ag diffusion from the metastable layer to the $Ge_{20}S_{80}$ host layer, and the third minimum corresponds to the uniform saturated reaction layer.

The metastable reaction layer seems to show a presence of a stable compound in the ternary system under a light illumination. In fact, Wagner and Frumar [52] proposed a formation of Ag_2S as an intermediate step in the photo-induced reaction, and successive changes to stable phases where glass-forming ability is high in Ag–As–S ternary system, although they did not assert the formation of Ag_2S in their following references [43, 44, 53]. The phase stability in the Ag–Ge–S system is different from that in the Ag–As–S system. However, the phase diagram of the Ag–Ge–S ternary system is similar to that of the Ag–Ge–Se ternary system [54–58]. In the Ag–Ge–S ternary system, Ag_2S is stable. Besides, Ag_8GeS_6 is also a stable compound [54, 55], which is known as a mineral called argyrodite. Its composition is closer compared to the metastable layer, which is $Ag_{0.69}(Ge_{0.2}S_{0.8})_{0.31}$. Ag_8GeS_6 can be regarded as a compound of $(Ag_2S)_4 + GeS_2$, and is built up with hexagonally arranged S atoms and triangularly arranged GeS_2 tetrahedral units [59]. Considering the valency of the atoms (Ag^+, Ge^{4+}, S^{2-}) and the neutrality of the compound, this composition should be stable. Additionally, GeS_6 ($Ge_{0.14}S_{0.86}$) has comparatively similar composition to $Ge_{20}S_{80}$. In the present case of silver photodiffusion, we infer that Ag ions dissolve into the $Ge_{20}S_{80}$ host matrix by a light exposure by forming a Ag_8GeS_6-type

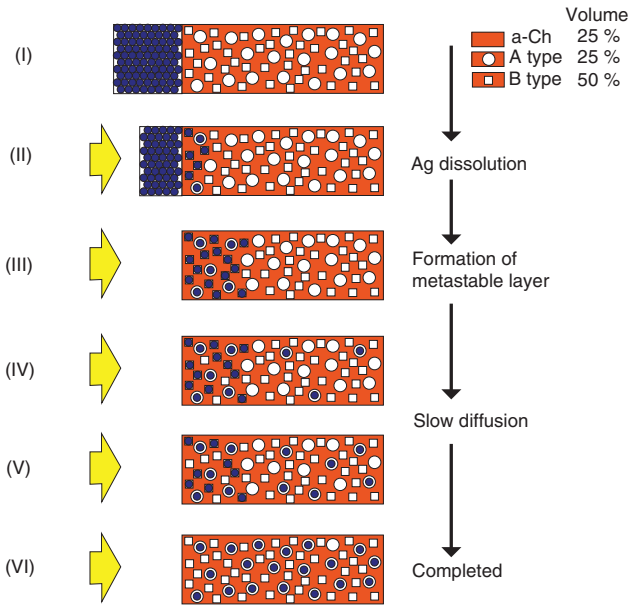

Fig. 11: Possible structural model of silver photodiffusion into amorphous $Ge_{20}S_{80}$, based on the concept of "*vacant sites*", which can capture Ag ions.

compound. In the compound, the S atoms, which are independent from the GeS_4 tetrahedral unit, capture Ag ions, as though the local Ag_2S units are formed. To form the compound, the host layer should be S-rich germanium sulphide which comparatively resembles $Ge_{0.14}S_{0.86}$. This makes sense because a formation of such metastable layer is observed only for S-rich amorphous germanium sulphide, and not observed in the case of stoichiometric composition and the Ge-rich composition [21, 22].

According to the intercalation model of silver photodiffusion proposed by Kluge [60], Ag ions are captured by chalcogen sites. The result of the present study on silver photodiffusion into S-rich germanium sulphide may be explained using the concept of "*vacant sites*", which can capture Ag ions, as shown in Fig. 11. Prior to light exposure, the film is composed of a Ag layer and a $Ge_{20}S_{80}$ layer (I). In the $Ge_{20}S_{80}$ layer, there are two types of vacant sites, *A* type and *B* type. For example, the volume fraction of the *A* type vacant sites is 25 %, while the volume fraction of the *B* type vacant sites is 50 %. By initiating the light exposure, Ag ions enter both *A* type vacant sites and *B* type vacant sites in the vicinity of the interface (II). Under continuous light exposure, all Ag ions in the Ag layer enter vacant sites (of *A* type and *B* type) in the vicinity of the surface, resulting in the disappearance of the Ag layer (III). In the surface region, almost all the vacant sites are occupied by Ag ions, and a uniform metastable reaction layer is formed. This reaction occurs very quickly. We assume here that the Ag ions in both the vacant sites diffuse only to the *B* type vacant sites with a longer reaction time (phase IV to phase V, in Fig. 11) until their distribution becomes homogeneous in the entire film (VI).

According to *ab initio* molecular dynamics simulations of $Ag_x(GeSe_3)_{1-x}$ (x = 0.10 and 0.15) by Tafen et al. [61], there are mobile and immobile Ag ions. This result indicates that there are two types of Ag capturing sites, and also indicates consistency with our model using the vacant sites. In addition, according to our recent structural study on Ge–S glasses, there are two types of covalent bonds in amorphous $Ge_{20}S_{80}$: a Ge–S bond and a S–S bond [62].These two bonds may be related to the two types of vacant sites in Fig. 11. For the metastable reaction layer, we assumed that the Ag_8GeS_6 type compound was formed. It is noted that Ag_8GeS_6 can be regarded as $(Ag_2S)_4(GeS_2)$ and that $Ge_{20}S_{80}$ can be regarded as $(Ge_{20}S_{40})S_{40} = (GeS_2)S_2$. The S atoms with the S–S bond in $Ge_{20}S_{80}$ are apart from the GeS_4 tetrahedral unit and could capture Ag ions to make the local Ag_2S type unit. In contrast, the composition of the saturated reaction layer is estimated to be $Ag_{0.34}(Ge_{0.2}S_{0.8})_{0.66} = Ag_{0.34}Ge_{0.13}S_{0.53}$. In the composition, Ag ions can be completely captured by two S atoms in the GeS_2 tetrahedral units. This means that the S atoms with the Ge–S bond capture Ag ions in the compound. These expectations may be proved by further structural studies of the Ag-diffused films.

Conclusion

We performed the time-resolved neutron reflectivity measurement of a Ag 500 Å/$Ge_{20}S_{80}$ 1500 Å/Si substrate and the optical reflectivity measurement of a Ag 500 Å/$Ge_{25}S_{75}$ 1500 Å/Si substrate to elucidate the kinetics of silver photodiffusion into amorphous S-rich germanium sulphide. In the neutron reflectivity measurement, the neutron reflectivity profiles with 30 s resolution were successfully obtained. It was found, based on the neutron reflectivity measurement, that there are two reaction processes. The first process is quick and concludes within 2 min. Ag dissolution occurs in the time region, forming a metastable reaction layer in the vicinity of the interface between the Ag layer and the $Ge_{20}S_{80}$ layer. The second process is comparatively slower and continues until 20 min. In the time region, Ag diffusion occurs from the metastable reaction layer to the $Ge_{20}S_{80}$ host layer. It was found, based on the optical reflectivity measurement, that a metastable reaction layer with metallic nature was formed in the initial fast reaction process within 2 min. The occurrence of the two reaction processes can be explained by assuming two types of vacant sites. Considering the structure of Ge–S glasses, the vacant sites are attributed to the nature of the bonds related to S atoms, being part of tetrahedral structures and connected to Ge, i.e. forming Ge–S bonding, or being part of S chains and forming S–S bonds. In the first process, Ag ions enter the germanium sulphide layer, and follows the S atoms around, which are independent of the GeS_4 tetrahedral units, as though Ag_2S-type units are formed in the Ag_8GeS_6-like compound. In the second process, Ag ions are expected to be captured by the S atoms which are contained in the GeS_4 tetrahedral units. The scenario is also consistent with the fact that the formation of the metastable layer is only observed in amorphous S-rich germanium sulphide. Such kinetics pictures on the silver photodiffusion may yield profound insight into the materials design of PMC devices or other new applications.

Acknowledgement: This research was supported by JSPS Grant-in-Aid for Scientific Research (C), Grant No. 25400435. The neutron reflectivity measurements were performed on BL17 (*SHARAKU*) at J-PARC MLF under Project No. 2013A0203. We would like to thank M. Ailavajhala (BSU) for the preparation of sample, Dr. T. Hanashima (CROSS), Dr. H. Aoki (JAEA) and S. Kasai (CROSS) for technical support on the neutron reflectivity measurement, K. Nakajima and T. Asano (Bunkoukeiki, Japan) for technical advices on the optical reflectivity measurement. We would like to thank Editage (www.editage.jp) for English language editing.

References

[1] A. V. Kolobov (Ed.), *Photo-Induced Metastability in Amorphous Semiconductors*, Wiley-VCH, Weinheim (2003).
[2] A. V. Kolobov, S. R. Elliott, *Adv. Phys.* **40**, 625 (1991).
[3] M. T. Kostyshin, E. V. Mikhailovskaya, P. F. Romanenko, *Fiz. Tverdogo Tela* **8**, 571 (1966) [*Sov. Phys.* (*Solid State*) **8**, 451 (1966)].
[4] A. Yoshikawa, O. Ochi, H. Nagai, Y. Mizushima, *Appl. Phys. Lett.* **29**, 677 (1976).
[5] J. Hajto, P. J. S. Ewen, R. E. Belford, A. E. Owen, *Thin Solid Films* **200**, 229 (1991).
[6] Y. Murakami, K. Arai, M. Wakaki, T. Shibuya, T. Shintaku, *Proc. SPIE* **9359**, 93591N (2015).
[7] M. Mitkova, M. N. Kozicki, *J. Non-Cryst. Solids* **299–302**, 1023 (2002).
[8] M. N. Kozicki, M. Mitkova, I. Valov, in *Resistive Switching: From Fundamentals of Nanoionic Redox Processes to Memristive Device Applications*, D. Ielmini, R. Waser, (Ed.), p. 483, Wiley, Weinheim (2015).
[9] Y. Yamamoto, T. Itoh, Y. Hirose, H. Hirose, *J. Appl. Phys.* **47**, 3603 (1976).
[10] J. Rennie, S. R. Elliott, C. Jeynes, *Appl. Phys. Lett.* **48**, 1430 (1986).
[11] G. Kluge, A. Thomas, R. Klabes, R. Grotzschel, P. Suptitz, *J. Non-Cryst. Solids* **124**, 186 (1990).
[12] R. E. Grandi, J. Calas, G. Galibert, M. Averous, *Thin Solid Films* **218**, 259 (1992).
[13] J. Calas, R. E. Grandi, G. Galibert, A. Traverse, *Nucl. Instrum. Methods Phys. Res. B* **63**, 462 (1992).
[14] T. Wagner, V. Perina, M. Vlcek, M. Frumer, E. Rauhala, J. Saarilahti, P. J. S. Ewen, *J. Non-Cryst. Solids* **212**, 157 (1997).
[15] T. Wagner, G. Dale, P. J. S. Ewen, E. Owen, V. Perina, *J. Appl. Phys.* **87**, 7758 (2000).
[16] A. Kovalskiy, A. C. Miller, H. Jain, M. Mitkova, *J. Am. Ceram. Soc.* **91**, 760 (2008).
[17] Y. Sakaguchi, H. Asaoka, Y. Uozumi, Y. Kawakita, T. Ito, M. Kubota, D. Yamazaki, S. K. M. Ailavajhala, M. R. Latif, M. Mitkova, *Can. J. Phys.* **92**, 654 (2014).
[18] Y. Sakaguchi, H. Asaoka, Y. Uozumi, Y. Kawakita, T. Ito, M. Kubota, D. Yamazaki, K. Soyama, M. Ailavajhala, M. R. Latif, K. Wolf, M. Mitkova, W. A. Skoda, *J. Phys.: Conf. Ser.* **619**, 012046 (2015).

[19] Y. Sakaguchi, H. Asaoka, Y. Uozumi, Y. Kawakita, T. Ito, M. Kubota, D. Yamazaki, K. Soyama, M. Ailavajhala, K. Wolf, M. Mitkova, M. W. A. Skoda, *JPS Conf. Proc.* **8**, 031023 (2015).
[20] Y. Sakaguchi, H. Asaoka, Y. Uozumi, Y. Kawakita, T. Ito, M. Kubota, D. Yamazaki, K. Soyama, G. Sheoran, and M. Mitkova, *Phys. Status Solidi A* **213**, 1894 (2016).
[21] Y. Sakaguchi, H. Asaoka, Y. Uozumi, K. Kondo, D. Yamazaki, K. Soyama, M. Ailavajhala, M. Mitkova, *J. Appl. Phys.* **120**, 055103 (2016).
[22] Y. Sakaguchi, H. Asaoka, M. Mitkova, *J. Appl. Phys.* **122**, 235105 (2017).
[23] Y. Sakaguchi, T. Hanashima, H. Aoki, H. Asaoka, Al-Amin A. Simon, M. Mitkova, *Phys. Status Solidi A* **215**, 1800049 (2018).
[24] O. S. Heavens, *Optical Properties of Thin Solid Films*, Butterworth, London (1955).
[25] D. S. Sivia, *Elementary Scattering Theory*, Oxford University Press, Oxford (2011).
[26] J. Daillant, A. Gibaud (Eds.), *Lecture Note in Physics 770, X-ray and Neutron Reflectivity Principles and Application*, Springer-Verlag, Berlin Heidelberg (2009).
[27] B. T. M. Willis, C. J. Carlile, *Experimental Neutron Scattering*, Oxford University Press, Oxford (2009).
[28] L. G. Parratt, *Phys. Rev.* **95**, 359 (1954).
[29] F. Abelès, *Le Journal de Physique et le Radium* **11**, 307 (1950).
[30] J. Als-Nielsen, D. McMorrow, *Elements of Modern X-ray Physics*, 2nd ed., Wiley, West Sussex (2011).
[31] M. Tolan, *X-ray Scattering from Soft-Matter Thin Films*, Springer-Verlag, Telos (1999).
[32] F. Bridou, J. Gautier, F. Delmotte, M.-F. Ravet, O. Durand, M. Modreanu, *Appl. Surf. Sci.* **253**, 12 (2006).
[33] K. Sakurai, M. Mizusawa, M. Ishii, *Trans. Mater. Res. Soc. Jpn.* **33**, 523 (2008).
[34] M. Takeda, D. Yamazaki, K. Soyama, R. Maruyama, H. Hayashida, H. Asaoka, T. Yamazaki, M. Kubota, K. Aizawa, M. Arai, Y. Inamura, T. Itoh, K. Kaneko, T. Nakamura, T. Nakatani, K. Oikawa, T. Ohhara, Y. Sakaguchi, K. Sakasai, T. Shinohara, J. Suzuki, K. Suzuya, I. Tamura, K. Toh, H. Yamagishi, N. Yoshida, T. Hirano, *Chin. J. Phys.* **50**, 161 (2012).
[35] S. Nagamiya, *Nucl. Instrum. Met. Phys. Res. B* **217**, 216 (2004).
[36] H. Takada, K. Haga, M. Teshigawara, T. Aso, S. Meigo, H. Kogawa, T. Naoe, T. Wakui, M. Ooi, M. Harada, M. Futakawa, *Quantum Beam Sci* **1**, 8 (2017).
[37] K. Sakasai, S. Satoh, T. Seya, T. Nakamura, K. Toh, H. Yamagishi, K. Soyama, D. Yamazaki, R. Maruyama, T. Oku, T. Ino, H. Kira, H. Hayashida, K. Sakai, S. Itoh, K. Suzuya, W. Kambara, R. Kajimoto, K. Nakajima, K. Shibata, M. Nakamura, T. Otomo, T. Nakatani, Y. Inamura, J. Suzuki, T. Ito, N. Okazaki, K. Moriyama, K. Aizawa, S. Ohira-Kawamura, M. Watanabe, *Quantum Beam Sci.* **1**, 10 (2017).
[38] The spectrum is found at: https://asahi-spectra.com/opticalinstrument/max350.html.
[39] R. K. Pan, H. Z. Tao, H. C. Zang, C. G. Lin, T. J. Zhang, X. J. Zhao, *J. Non-Cryst. Solids* **357**, 2358 (2011).
[40] T. Nakatani, Y. Inamura, K. Moriyama, T. Ito, S. Muto, T. Otomo, *JPS Conf. Proc.* **1**, 014010 (2014).
[41] A. Nelson, *J. Appl. Crystallogr.* **39**, 273 (2006).
[42] J. Strong, *Procedures in Experimental Physics*, pp. 375–376, Prentice-Hall, Inc., New York (1938).
[43] T. Wagner, M. Vlček, V. Smrčka, P. J. S. Ewen, A. E. Owen, *J. Non-Cryst. Solids* **164–166**, 1255 (1993).
[44] T. Wagner, E. Márquez, J. Fernández-Pena, J. M. González-Leal, P. J. S. Ewen, S. O. Kasap, *Phil. Mag. B* **79**, 223 (1999).
[45] L. Červinka, L. Tichý, J. Bergerová, *J. Non-Cryst. Solids* **232–234**, 335 (1998).
[46] S. R. Elliott, *J. Non-Cryst. Solids* **130**, 85 (1991).
[47] Y. Murakami, M. Wakaki, *Thin Solid Films* **542**, 246 (2013).
[48] T. Wagner, *J. Optoelectron. Adv. Mater.* **4**, 717 (2002).
[49] The optical absorption data of amorphous $Ge_{25}S_{75}$ were estimated from those of amorphous GeS_2 ($Ge_{33}S_{67}$) and GeS_4 ($Ge_{20}S_{80}$) in Ref. 39.
[50] M. Fox, *Optical Properties of Solids*, p. 143, Oxford University Press, Oxford (2001).
[51] G. B. Irani, T. Huen, F. Wooten, *Phys. Rev. B* **3**, 2385 (1971).
[52] T. Wágner, M. Frumar, *J. Non-Cryst. Solids* **116**, 269 (1990).
[53] T. Wagner, M. Frumar, in *Photo-induced Metastability in Amorphous Semiconductors*, A. V. Kolobov (Ed.), p. 161, Wiley-VCH, Weinheim (2003).
[54] G. Petzow, G. Effenberg (Eds.), V.2: Ag-Cu-Pb to Ag-Zn-Zr, in *Ternary Alloys; Comprehensive Compendium of Evaluated Constitutional Data and Phase Diagram*, p. 189, VCH, Weinheim (1988).
[55] O. Gorochov, *Bull. Soc. Chim. France* **6**, 2263 (1968).
[56] T. Kawaguchi, S. Maruno, S. R. Elliott, *J. Appl. Phys.* **79**, 9096 (1996).
[57] M. Mitkova, Y. Wang, P. Boolchand, *Phys. Rev. Lett.* **83**, 3848 (1999)
[58] Y. Wang, M. Mitkova, D. G. Georgiev, S. Mamedov, P. Boolchand, *J. Phys.:Condens. Matter* **15**, S1573 (2003).
[59] G. Eulenberger, *Monatsh. Chem.* **108**, 901 (1977).
[60] G. Kluge, *Phys. Stat. Sol. A* **101**, 105 (1987).
[61] De Nyago Tafen, D. A. Drabold, M. Mitkova, *Phys. Rev. B* **72**, 054206 (2005).
[62] Y. Sakaguchi, T. Hanashima, K. Ohara, Al-Amin A. Simon, M. Mitkova, *Phys. Rev. Mater.* **3**, 035601 (2019).